TIGHTLY-COUPLED INTEGRATION OF BLE AND PDR USING GRAPH OPTIMIZATION FOR INDOOR PEDESTRIAN NAVIGATION

Xuan Wang[1] , Yuan Zhuang[1, 3, *], Zhenghua Zhang[2], Xiaoxiang Cao[1], Xiansheng Yang[1]

[1] State Key Laboratory of Information Engineering in Surveying, Mapping and Remote Sensing, Wuhan University, Wuchang District, Wuhan 430079, China. (e-mail: 2021106190015@whu.edu.cn (X. Wang)
[2] School of Environmental and Spatial Informatics, China University of Mining and Technology, Xuzhou 221100, China.
[3] Wuhan Institute of Quantum Technology, Wuhan 430206, China.

Commission III, WG III/1

KEY WORDS: Indoor positioning, tightly-coupled integration, particle filter, graph-based optimization, pedestrian dead reckoning, Bluetooth low energy.

ABSTRACT:

In this paper, we propose an indoor navigation method based on the tightly-coupled (TC) integration of Bluetooth low energy (BLE) and pedestrian dead reckoning (PDR) using a graph optimization model. We first utilize the Gaussian probability model to update the particle weights that considers the ranging model's estimation performance at different distances to determine the particle weight. Moreover, the BLE walking-surveyed or crowdsourced landmarks, combined with accurate ranging of BLE at a short distance, is used to construct a graph optimization model, and the Levenberg-Marquardt (LM) algorithm is adopted to optimize this model to improve track tracking performance. The performance of the proposed algorithm has been verified in the hallway scene and another challenging room scene. The results show that compared with the standard particle filter (PF) method, the average positioning accuracy of the proposed algorithm is improved by 64.0% and 54.75%, and the error variance is significantly reduced by 76.23% and 68.60%, respectively, which is a significant improvement in both robustness and accuracy. Furthermore, the test shows that the proposed method can calculate reasonable trajectories even in complex room scenarios.

1. INTRODUCTION

Recently, with the popularisation of intelligent equipment and the construction of ubiquitous sensor networks, digital cities, smart homes, the internet of things, people have an increasingly urgent demand for indoor positioning (Wang et al., n.d.). Due to the signal obstruction and multipath effects, mature satellite positioning technology is difficult to provide reliable positioning services indoors. It is extremely challenging to find an accurate and stable indoor positioning method. Fortunately, abundant sensors deployed in the environment and powerful sensor systems mounted on mobile platforms such as smartphones, constitute a wireless sensor network providing conditions for indoor positioning implementation. Scholars have explored numerous indoor positioning technologies such as inertial navigation systems (INS) (Chen et al., 2021, Chen et al., 2020), BLE (Baronti et al., 2018, Choi et al., 2022), WiFi (Ji et al., 2022, Ko and Wu, 2022), magnetic (Wang et al., 2022, Wang et al., 2016), ultra-width band (UWB) (Bing et al., 2018), sound (Liang et al., 2018), and visible light positioning (Zhuang et al., 2019). Although the mainstream technologies have their advantages, they also have limitations. The UWB, light emitting diode (LED), ultrasonic, infrared, and pseudo satellites are limited by an expensive foundation and implementation environments. WiFi, Bluetooth, and geomagnetic positioning face uncertain environment interference and received signal strength (RSS) fluctuation. Inertial navigation positioning is also limited by error accumulation. Thus, multi-sensors fusion is the realistic solution according to various works.

Frank et al. (Korbinian et al., 2009) proposed a pedestrian navigation solution based on WiFi fingerprinting with a magnetometer and foot-mounted inertial sensors, which is a foot-mounted system not suitable for handheld devices. Mamun et al. (Lee et al., 2017) combined the micro-electromechanical systems (MEMS)-based PDR with the RSS-based fingerprinting method to perform position estimates, and the indoor floor plan was utilized to implement a landmark-assisted PDR. However, fingerprint positioning is labour-intensive and is not conducive to system maintenance and upgrade. Zhuang et al. (Zhuang and El-Sheimy, 2016) presented a tightly-coupled integration system of WiFi and MEMS sensors to improve the performance in an environment with the sparse deployment of APs. Furthermore, a two-filter fusion for MEMS and WiFi fingerprint was proposed in their another work to constrain the search space and achieve a constrained solution (Zhuang et al., 2016). Two other methods of using propagation models to fuse IMU were proposed in (Yu et al., 2017), and both reported positioning accuracy greater than 3 m. Moreover, a WiFi time of flight (ToF) indoor positioning system with MEMS-based INS was proposed in (Schatzberg et al., 2014), but current universally installed WiFi chipsets do not support ToF. Moreover, some fusion schemes such as IMU/UWB (Krishnaveni et al., 2021), IMU/Camera (Poulose and Han, 2019) and IMU/Audio/Bluetooth (Xu et al., n.d.) have been prosperous in recent years, but these schemes often rely on additional expensive device hardware and face many problems such as the multipath and the light-of-sight (NOL). This paper mainly focuses on the ubiquitous BLE and IMU positioning technologies and uses a tight combination and graph optimization technique to achieve a robust and robust integration system.

BLE improves the Bluetooth technology with a low energy consumption and a long lifetime, which has been widely used since they perform better in terms of quality and cost. PDR, especially on smartphones, is a method of inertial navigation that also plays an increasingly important role in indoor navigation due to its continuous positioning, fast data updating, and the ability to work

*Corresponding author. E-mail: yuan.zhuang@whu.edu.cn (Y. Zhuang)

without additional hardware. Thus, in this paper, we propose an indoor navigation method based on the TC integration of BLE and PDR. In order to make the smartphone-based navigator accurate and practical, we proposed two methods to improve the navigation performance:

1. The first approach utilizes the PF algorithm to perform a TC fusion of BLE and PDR. Different from the study (Zhuang and El-Sheimy, 2016), which uses EKF to integrate the MEMS and the distance converted by RSS, we innovatively propose a Gaussian-based distance model (GDM) to update the particle weights to reduce the adverse effects of the inaccuracy range model and instability of signals at different distances (in particular, propagation model accuracy loss in the middle and long-distance (Qureshi et al., 2019)). Moreover, the proposed TC fusion model can reduce PDR's drift by using BLE information even if only one or two access points (APs) are available.
2. In the second approach, we leverage the advances of the pose-graph-based optimization techniques and the simultaneous localization and mapping techniques. In our proposed system, the graph constraints are constructed by multiple information, including the pose graph, the RSS of the BLE, the updated position, the heading and step information calculated by the PDR construction, and the signal or behavioural landmark information. After the graph is constructed, the PDR system and position estimation are optimized.

The rest of this article is organized as follows. In Section 2, PDR-based navigation and the proposed GDM-based BLE are described. Then, the TC integration of PDR and BLE is presented. The graph optimization model is discussed and proposed. The experimental results are presented in Section 3, and the conclusions and future work are summarized in Section 4.

2. BDM-BASED BLE AND PDR NAVIGATION

2.1 PDR-Based Navigation

PDR is a localization algorithm suitable for low-cost microelectronic systems since it does not depend on infrastructure and high-precision hardware. PDR periodically updates the position using the heading and step length information obtained from the inertial sensors.

This paper adopts a robust step counting method proposed in our previous work (Wang et al., n.d.) to perform pedestrian step detection and eliminate incorrect position updates in non-walking states. Step length estimation algorithm adopts a Weinberg model commonly used in PDR, which uses the difference between each step cycle's maximum and minimum acceleration to determine the step length. The model is as follows:

$$L = k \cdot \sqrt[4]{Acc_{\max} - Acc_{\min}}, \tag{1}$$

where, $Acc_{\max}$ and $Acc_{\min}$ are the maximum and minimum vertical accelerations, respectively, and the constant k is set as 0.35 by testing pedestrians with different heights.

The attitude and heading reference system (AHRS) is an attitude reference system that has strong robustness and high accuracy due to the fusing of the accelerometer, gyroscope, and magnetometer data. In this study, the Madgwick-AHRS (Madgwick and Others, 2010) algorithm is adopted to obtain the device's attitude held by the user.

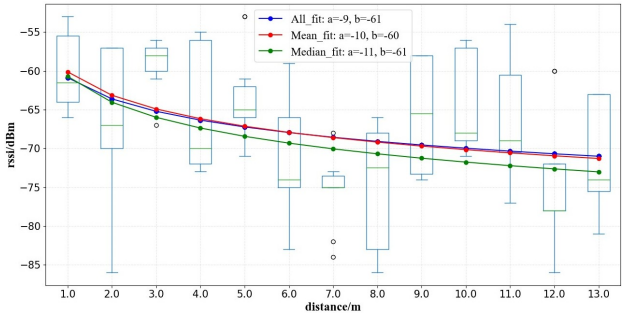

Figure 1: The collected data are used to fit the signal propagation model.

In the PDR system, it is assumed that the initial position is recorded as $(\mathrm{x}_{k-1}, \mathrm{y}_{k-1})$, the following formula can generally express the recursive form at the next moment:

$$\begin{pmatrix} x_k \\ y_k \end{pmatrix} = \begin{pmatrix} x_{k-1} \\ y_{k-1} \end{pmatrix} + \Delta r_{k-1} \times \begin{pmatrix} \cos\theta_{k-1} \\ \sin\theta_{k-1} \end{pmatrix}, \tag{2}$$

where Δr_{k-1} represents the single step size calculated by the step detection algorithm, and the θ_{k-1} represents the heading for this step.

2.2 BLE base on Gaussian-based distance model

The typical propagation model follows the distance power law:

$$RSSI = A - 10 \cdot n \cdot \lg d + X_\sigma, \tag{3}$$

where $RSSI$ represents the estimation of received signal strength at a distance from the transmitter; A is a constant that represents RSS at 1m from the transmitter; N represent the path loss exponent with typical values; X_σ represents the noise modeled as a Gaussian random variable with zero mean. The distances between the receiver and the AP can be calculated by the following formula:

$$d = \frac{A - RSSI}{10 \cdot n}, \tag{4}$$

where A and n are constants generally fitted with a large amount of data collected at different distances.

As shown in Figure 1, the logarithm-normal distribution propagation model fitted to all data, mean, and median at different distances describes the relationship between spatial distance and signal strength to a certain extent. However, due to the hardware characteristics and complex indoor environment, this method still faces signal uncertainty, non-line-of-sight, and insufficient ranging accuracy in medium and long distances about of 5-15 m. The RSS at different distances can be described by:

$$\overline{RSSI_{Di}} = RSSI_{Di} + X_\sigma^{Di}, \tag{5}$$

where $RSSI_{Di}$ represents the $RSSI$ observation at distance i , and the $RSSI_{Di}$ represents the true RSSI at the corresponding position. The RSSI noise can be modelled as Gaussian noise (Salo et al., 2007, Kschischang et al., 2001), i.e., $X_\sigma^{Di} \sim \left(0, \sigma_{Di}^2\right)$. Thus, we can assume that the $RSSI_{Di} \sim \left(u_{Di}, \sigma_{Di}^2\right)$ at distance Di from the transmitter, and the u_i and the σ_{Di}^2 can be calculated by the signals collected at different distances. Compared with the fitted logarithmic curve, the mean and variance variables can better describe the signal strength and the fluctuation characteristics of the signal at different distances and provide support for the next TC integration and gross error detection.

2.3 System Model of TC Integration

This section describes the TC of PDR and BLE in detail. In this paper, a TC model is constructed based on the PF algorithm, which utilizes the PDR algorithm to update the particle state and the particle weight update by GDM defined in the previous section rather than the BLE-based ranging model. The advantage of the TC is that the BLE can be utilized to reduce PDR error accumulation in the case of fewer than three transmitters. The proposed TC model performs better than the loosely-coupled integration and reduces the adverse effects of inaccurate ranging models and varying signal fluctuations at different distances on fusion systems.

The basic process of particle filtering includes four parts: initialization, importance sampling, weight calculation, and resampling. The particle's initial position $\left(\mathrm{x}_0^i, y_0^i\right)$ follows the Gaussian distribution and the mean of the particles is the mean of the multiple BLE location results. The following equation gives the system variables and their updates:

$$X_t = S\left\{X_t^i \mid i = 1, 2, \ldots, n\right\}, \tag{6}$$

$$X_t^i = \left(x^i, y^i, \theta^i\right)^T, \tag{7}$$

in which,S represents the set of particles at time t, and X_t^i represent the position and heading of the particle at time t. Every particle can be recurrence as fellow:

$$X_{t+1} = \begin{bmatrix} x_{t+1} \\ y_{t+1} \\ \theta_{t+1} \end{bmatrix} = \begin{bmatrix} x_t + l_t \times \cos\theta_t \\ y_t + l_t \times \sin\theta_t \\ \theta_t + \Delta\theta_{t:t+1} \end{bmatrix} + W_{t-1}^{3\times 1}, \tag{8}$$

where l_{t-1} and $\Delta\theta_{t:t+1}$ are the variation of pedestrian step length and pedestrian heading estimated by the step detection algorithm, respectively. The updated state vector of a particle can be expressed as:

$${X_{t+1}^i}' = \left(x^i, y^i, \theta^i\right)^T, \tag{9}$$

The particle's weight can be calculated by the GDM model established in the previous section. The algorithm first calculates the actual distance between the updated particle and each AP:

$$d_{AP,k}^i = \sqrt{\begin{array}{l}\left[\left(\lambda_{Xi} - \lambda_{AP,k}\right)(N+h)\cos\varphi\right]^2 \\ +\left[\left(\varphi_{Xi} - \varphi_{AP,k}\right)(M+h)\right]^2\end{array}}, \tag{10}$$

where λ_{Xi} and φ_{Xi} represent the longitude and latitude in the geodetic coordinate system corresponding to the PDR-based particle position; M and N represent the meridian radius and prime vertical of the earth curvature, respectively; $\lambda_{AP,k}$ and $\varphi_{AP,k}$ represent position coordinates of the kth BLE AP. Therefore, bringing the $d_{AP,k}^i$ of each particle and the $RSSI_{AP,k}$ into the Gaussian model, the sum of the probability of the particle can be calculated and used as particle weights:

$$w^i = \begin{cases} 0, \left|RSSI_{AP,k=1,2\cdots} - u_{d'\approx d_{AP,k=1,2,\cdots}^i}\right| > 3\sigma_{d'\approx d_{AP,k=1,2,\cdots}^i} \\ \sum\limits_{k=1}^{n=N_{AP}} \frac{1}{\sqrt{2\pi}\sigma} e^{-\frac{\left(RSSI_{AP,k} - u_{d'\approx d_{AP,k}^i}\right)^2}{2\sigma^2_{d'=d_{AP,k}^i}}}, \text{other} \end{cases} \tag{11}$$

where $RSSI_{AP,k}$ represents the observed $RSSI$ of $k-th$ AP. When building the GDM model, We build several Gaussian-distributed signal models at approximately 0.5m intervals over a distance of 0.5m -15m. Thus, $d' \approx d_{AP,\mathrm{k}}^i$ represent the algorithm would bring the RSSI into the nearest signal strength probabilistic model. Moreover, the algorithm also introduces the "3σ" criterion to exclude some incorrect particle updates. Then, the fusion system output position is given by Equation 12:

$$P = \sum_{i=1}^{n} w_i \left(x^i, y^i\right)^T. \tag{12}$$

2.4 Graph optimization model based on LM algorithm

Factor graph was first proposed in (Kschischang et al., 2001) to model factorizations. Formally, a graph contains two types of nodes, namely variable nodes and factor nodes, and the edges. Variable nodes represent state variables at different movements, and the edge connects the variables nodes and factor nodes, which encodeS the error function. An error function represents a probability constraint applied to a state, and the goal is to find an optimal state that minimises the sum of all error functions. The optimization graph can be expressed as:

$$X = \min_{X_0} \varepsilon^T w \varepsilon \tag{13}$$

where X represents the space state quantity to be optimized in the graph; ε represents the error function; w represents the weights of the constraints of the entire optimization problem. An optimal state estimate can be computed using a traditional nonlinear least-squares formulation, thereby minimizing the error on the graph, a least-squares optimization problem since it seeks to minimise the sum of squares.

Matched behavioral landmark (MBL) (Wu et al., n.d.), matched signal landmark (MSL), and the ranging information are utilized as the constraints of the factor graph. The MBL refers to the behavioral or location landmarks detected by methods such as machine learning, sensor thresholds detection, or deep learning, which are directly mapped to the location of an entity. The MSL refers to the signals landmarks collected by walking-surveyed or crowdsourcing. As shown in Figure 2, the PDR trajectory can be divided into several segments by the MBL and MSL, and the end position of every segment can be estimated by:

$$P_L = \begin{pmatrix} x_l \\ y_l \end{pmatrix} = P_{k_0} + \sum_{k=k_0}^{l} \Delta r_{k-1} \times \begin{pmatrix} \cos\theta_{k-1} \\ \sin\theta_{k-1} \end{pmatrix} \tag{14}$$

in which, P_L and P_{k_0} represent the start-point and the end-point position calculated by PDR, respectively; l is the step number of the trace. Thus, system accumulated deviation is resulted from the inaccurate step length and heading estimation, and the state can be expressed as:

$$\begin{aligned} X_0 = &[\Delta r_{k_0}, \Delta r_{k_0+1}, \Delta r_{k_0+2}, \ldots, \Delta r_{k-1} \\ &\theta_{k_0}, \theta_{k_0+1}, \theta_{k_0+2}, \ldots, \theta_{k-1}] \\ &\text{where }, \Delta r_k \geq 0, \pi > \theta_k > -\pi \end{aligned} \tag{15}$$

Figure 2 illustrates the basic concept of graph-based optimization utilizing the three constraints mentioned above. First, the basic observations of the PDR recursive system generate the graph nodes. Then, when the system detects MBL or MSL, it will detect the most recent steps and extract the last optimization key position to form an optimization sequence. Finally, the accumulated error is reduced by the constraints of the geographic location $\mathrm{MBL} \rightarrow Z_p$ or $\mathrm{MSL} \rightarrow Z_p$, and the distance calculated by the

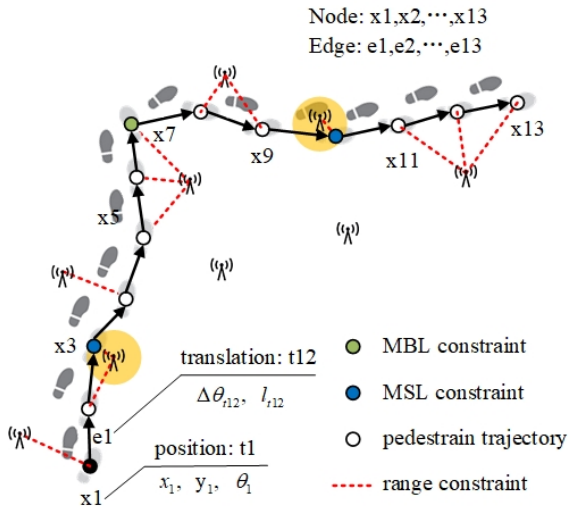

Figure 2: Illustration of the proposed graph model mainly includes three constraints: MBL, MSL, and range measurement.

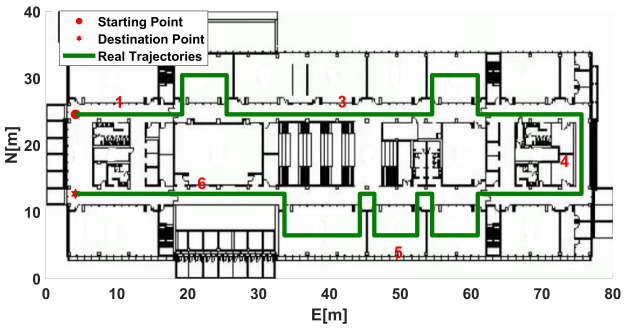

Figure 3: Ichnography and trajectories for the test scene.

strongest RSSI. A cost function can be defined as:

$$\varepsilon = f(\hat{x}) \triangleq \left\{ \left\| P_{k_0} + \sum_{k=k_0}^{l} \Delta r_{k-1} \times \begin{pmatrix} \cos\theta_{k-1} \\ \sin\theta_{k-1} \end{pmatrix} - Z_p \right\|_{w1} + \left\| \sum_{m=1}^{N_{ap}} \sum_{k=k_0}^{l} \left| \mathrm{D}_{pm}^{k} - \mathrm{D}_{ap-p}^{k} \right| \right\|_{w2} \right\},$$

$$\text{where} \left\{ \begin{array}{l} D_{ap-p}^{l} = 10^{-\frac{RSSI_l^m + A}{10 \times n}} \\ D_{pm}^{l} = \sqrt{\begin{array}{l} (\lambda_{Xi} - \lambda_{AP,\,\mathrm{m}})(N+h)\cos\varphi \\ +\left[(\varphi_{Xi} - \varphi_{AP,\,\mathrm{m}})(M+h)\right]^2 \end{array}} \end{array} \right\} \tag{16}$$

in which, w_1 and w_2 represent the weightS of two types of constraints. The closer to the end of the sequence, the higher weight will be for the weight w_1. While w_2 is regarded as an equal weight estimation. As the range estimation accuracy significantly reduced with increasing distance, we only adopted the strongest RSSI observations at each step as constraints.

We introduce the LM algorithm to solve this nonlinear least-squares optimization problem. The Second-order Taylor expansion of the cost function equation is as follows:

$$\begin{aligned} f(X) \approx & f(X_0) + \left(J(X_0)^T \times \psi_0 \right)^T \times \delta_X \\ & + \frac{1}{2} \delta_X^T \times \left(J(X_0)^T \times J(X_0) + \mu I \right) \times \delta_X \end{aligned} \tag{17}$$

where X_0 is the function expansion point; J is the Jacobi matrix of Equation 16; μ is the second-order information term omitted in the Gauss-Newton algorithm. LM is an iterative solution process. The iteration $k-th$ is as follows:

$$\begin{aligned} X_{k+1} = X_k - & \left(J(X_k)^T J(X_k) + uI \right)^{-1} \\ & \times J(X_k)^T \cdot f(X_k) \end{aligned} \tag{18}$$

The LM can be utilized to fuse the MBL, MSL, and RSSI observation with the model above to optimize the PDR estimation.

3. EXPERIMENTAL RESULTS

Our previous work evaluated that the tight-coupled model improved the performance of the MEMS-based positioning even if less than 3 APs (Zhuang and El-Sheimy, 2016), so we did not repeatedly evaluate it in this work. In this study, to evaluate the performance of the proposed indoor pedestrian navigator, sever experiments were performed. The experiment site prototype was the university of Calgary building E, with a floor area of approximately 3200 m^2. We mainly evaluated the positioning performance of the tightly-coupled PF based on map match (MPF), the proposed tightly-coupled PF based on map match and graph optimization (OMPF), standard PF, PDF, and BLE. Our previous work (Wang et al., 2020) has exhaustively evaluated the relationship between the number of particles, the positioning accuracy, and the calculation cost in detail. The results show that when the number of particles exceeds 200, the system's positioning accuracy tends to be stable. Therefore, the particle number is set to 200 in the proposed PF algorithm. As shown in Figure 3, a challenging trajectory was designed to evaluate the performance of the proposed methods. In this case, test data were simulated in the corridors and room environments, and wireless signals of about 27 APs were simulated for positioning.

The positioning results of the trajectories are shown in 4 and Table 1. This challenging trajectory traverses the corridor and the room scene, and its complex interior structure results in poor signal quality and great difficulty in particle updating. The results clearly show that the PDR positioning can continuously track the pedestrian position but is limited by the serious error accumulation, the mean positioning error is 6.01 m, and the maximum positioning error in the north direction (MEND) reaches 9.00 m. There is no errors accumulation in BLE positioning, but it faces serious problems such as positioning result rollback, dense/sparse positioning results, and poor positioning continuity. The mean errors (ME) and maximum positioning errors in the east direction (MEED) of BLE are 1.81 m and 5.20 m, respectively. The standard PF performs greatly decreasing rationality of updated trajectory, which is difficult to consistent with the real situation due to the more complex indoor structure. In the testing process, the method that only uses the building structure to restrict the particle updating and the methods would repeatedly face the problem of particle update failure, i.e., the particle cannot enter or leave a room which significantly reduces the localization performance. As shown in Figure 4, compared with the standard PF algorithm, the ME of the MPF algorithm is reduced by 55.93%, and the positioning stability is improved by 70.25%. The results indicate that the proposed MPF can solve the above problem and significantly improve the localization performance and rationality.

We introduced this approach into the MPF and evaluated the proposed OMPF in testing trajectory. The performance comparisons of MPF and OMPF are shown in Figure 5, and the navigation performances are summarized in Table 2. We can find that the OMPF

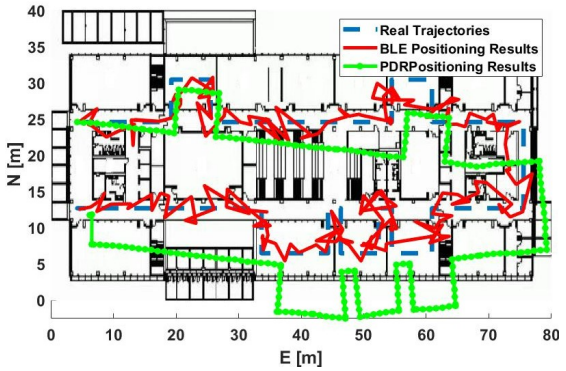

(a)

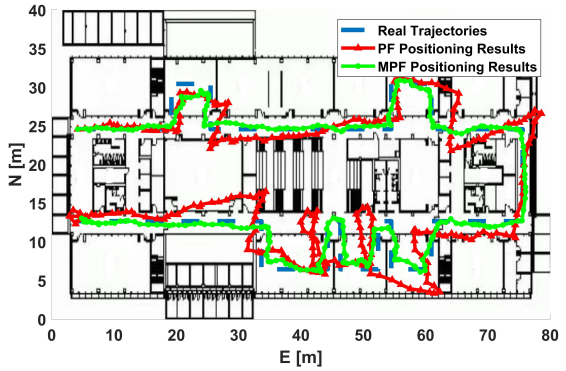

(b)

Figure 4: Positioning results of BLE, PDR, PF, and MPF for the first trajectory with a total length of approximately 230 m: (**a**) the positioning performance of BLE and PDR and (**b**) the positioning performance of PF and MPF.

	ME(m)	EV(m)	MEED(m)	MEND(m)
BLE	1.81	1.24	5.20	4.17
PDR	6.01	6.80	3.78	9.00
PF	2.36	1.21	4.49	3.82
MPF	**1.04**	**0.36**	**2.83**	**3.06**

Table 1: The positioning results of the second trajectory.

further improves the accuracy of pedestrian trajectory, especially at the corners and the edge of the building and room. In particular, when the algorithm matches MBL or MSL, the system would re-initialise the particle. This measure can avoid divergence of the longer-time particle filter system and helps the system to work over a long time. The OMPF further reduces the ME to about 0.9 m, and the positioning accuracy is further improved by 11.54% compared with the MPF methods, which also shows that OMPF has more obvious advantages in complex scenarios. As shown in Figure 6, the cumulative error percentages for a different approach also indicate the significant improvement of the proposed approach.

	ME(m)	EV(m)	MEED(m)	MEND(m)
PF	2.36	1.21	4.49	3.82
MPF	1.04	**0.36**	**2.83**	3.06
OMPF	**0.92**	0.38	3.45	**3.05**

Table 2: Comparisons of navigation performance for PF, MPF, and OMPF.

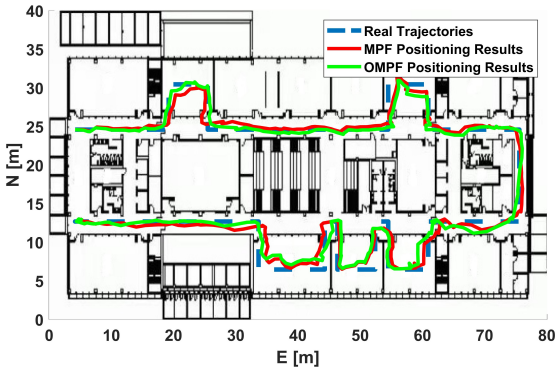

Figure 5: Navigation solutions of MPF and OMPF

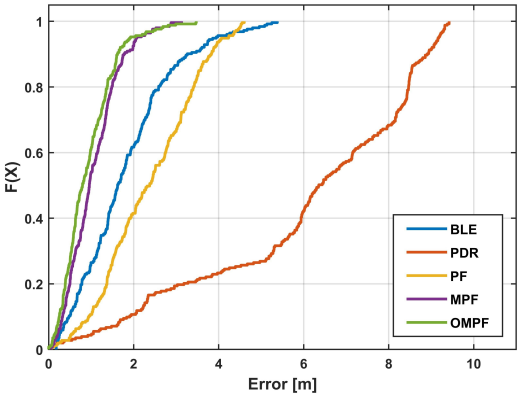

Figure 6: Cumulative error percentages of BLE, PDR, PF, MPF, and OMPF

4. CONCLUSION

This study presented a handheld indoor positioning navigator and proposed two major contributions to improve the accuracy and robustness of this navigator. Firstly, a PF was constructed to perform a TC model of BLE/PDR, and a GDM was innovatively proposed updating the particle weights. Moreover, we leveraged the advanced application of graph optimization within the robotics field to propose a graph optimization model that extensively used the wireless signal RSS, the matched MBL/MSL as constraints to optimize the PDR system and position estimation. Experimental results showed that the proposed MPF and OMPF had better accuracy and robustness than existing solutions, especially when dealing with the problem of insufficient positioning accuracy and unreasonable trajectory update in some complex scenes. Besides, in this study, information such as wireless signals, behavioral landmarks, and the architecture structure was used as a restriction to optimize systems, and one room and corridor scene were used to test the proposed system. More information (such as light, barometric pressure, magnetic field, velocity), more environments (such as shopping malls, workshops, transportation hubs), and more advanced error models will be studied and tested further in future works.

ACKNOWLEDGEMENTS

This work was partly supported by Excellent Youth Foundation of Hubei Scientific Committee (2021CFA040) and and Hubei Province International Science and Technology Collaboration Program (2021EHB012) and Guangdong Basic and Applied Basic Research Foundation (2021A1515110343) and the Fundamental Research Funds for the Central Universities (2021ZDPY0220).

REFERENCES

Baronti, P., Barsocchi, P., Chessa, S., Mavilia, F. and Palumbo, F., 2018. Indoor bluetooth low energy dataset for localization, tracking, occupancy, and social interaction. Sensors.

Bing, W., Yanyan, L., Qingquan, L. and Yan, Z., 2018. A high-precision dynamic indoor localization algorithm based on uwb technology. In: 2018 Ubiquitous Positioning, Indoor Navigation and Location-Based Services (UPINLBS), IEEE, pp. 1–7.

Chen, C. H., Lu, C., Wahlstrom, J., Markham, A. and Trigoni, N., 2021. Deep neural network based inertial odometry using low-cost inertial measurement units. IEEE Transactions on Mobile Computing 20(4), pp. 1351–1364.

Chen, C. H., Zhao, P. J., Lu, C. X., Wang, W., Markham, A. and Trigoni, N., 2020. Deep-learning-based pedestrian inertial navigation: Methods, data set, and on-device inference. IEEE Internet of Things Journal 7(5), pp. 4431–4441.

Choi, J., Lee, G., Choi, S. and Bahk, S., 2022. Smartphone based indoor path estimation and localization without human intervention. IEEE Transactions on Mobile Computing 21(2), pp. 681–695.

Ji, Y., Zhao, X., Wei, Y. and Wang, C., 2022. Generating indoor wi-fi fingerprint map based on crowdsourcing. Wireless Networks pp. 1–13.

Ko, C. H. and Wu, S. H., 2022. A framework for proactive indoor positioning in densely deployed wifi networks. IEEE Transations on Mobile Computing 21(1), pp. 1–15.

Korbinian, F., Krach, B., Catterall, N. and Robertson, P., 2009. Development and evaluation of a combined wlan & inertial indoor pedestrian positioning system. In: Proceedings of the 4th International Symposium on Location and Context Awareness, Savannah, GA, USA, pp. 22–25.

Krishnaveni, B. V., Reddy, K. S. and Reddy, P. R., 2021. Indoor tracking by adding imu and uwb using unscented kalman filter. Wireless Personal Communications.

Kschischang, F. R., Frey, B. J. and Loeliger, H. A., 2001. Factor graphs and the sum-product algorithm. IEEE Transactions on Information Theory 47(2), pp. 498–519.

Lee, M. S., Ju, H. and Park, C. G., 2017. Map assisted pdr/wi-fi fusion for indoor positioning using smartphone. International Journal of Control Automation & Systems.

Liang, X., Wang, G. and Han, Z., 2018. A low-cost collaborative indoor localization system based on smartphone platform. In: 2018 IEEE International Conference on Internet of Things (iThings) and IEEE Green Computing and Communications (GreenCom) and IEEE Cyber, Physical and Social Computing (CPSCom) and IEEE Smart Data (SmartData), IEEE, pp. 404–411.

Madgwick, S. and Others, 2010. An efficient orientation filter for inertial and inertial/magnetic sensor arrays. Report x-io and University of Bristol (UK) 25, pp. 113–118.

Poulose, A. and Han, D. S., 2019. Hybrid indoor localization using imu sensors and smartphone camera. Sensors.

Qureshi, U. M., Umair, Z. and Hancke, G. P., 2019. Evaluating the implications of varying bluetooth low energy (ble) transmission power levels on wireless indoor localization accuracy and precision. Sensors 19(15), pp. 3282–.

Salo, J., Vuokko, L., El-Sallabi, H. M. and Vainikainen, P., 2007. An additive model as a physical basis for shadow fading. IEEE Transactions on Vehicular Technology 56(1), pp. 13–26.

Schatzberg, U., Banin, L. and Amizur, Y., 2014. Enhanced wifi tof indoor positioning system with mems based ins and pedometric information. In: Proceedings of IEEE/ION PLANS 2014, pp. 185–192.

Wang, L. Y., Luo, H. Y., Wang, Q., Shao, W. H. and Zhao, F., 2022. A hierarchical lstm-based indoor geomagnetic localization algorithm. IEEE Sensors Jouranl 22(2), pp. 1227–1237.

Wang, S., Wen, H., Clark, R. and Trigoni, N., 2016. Keyframe based large-scale indoor localisation using geomagnetic field and motion pattern. In: 2016 IEEE/RSJ international conference on intelligent robots and systems (IROS), IEEE, pp. 1910–1917.

Wang, X., Chen, G., Cao, X., Zhang, Z., Yang, M. and Jin, S., n.d. Robust and accurate step counting based on motion mode recognition for pedestrian indoor positioning using a smartphone. IEEE Sensors Journal pp. 1–1.

Wang, X., Chen, G., Yang, M. and Jin, S., 2020. A multi-mode pdr perception and positioning system assisted by map matching and particle filtering. International Journal of Geo-Information 9(2), pp. 93.

Wu, Y., Chen, R., Li, W., Yu, Y., Zhou, H. and Yan, K., n.d. Indoor positioning based on walking-surveyed wi-fi fingerprint and corner reference trajectory-geomagnetic database. IEEE Sensors Journal 21(17), pp. 18964–18977.

Xu, S., Chen, R., Guo, G., Li, Z., Qian, L., Ye, F., Liu, Z. and Huang, L., n.d. Bluetooth, floor-plan, and mems assisted wide-area audio indoor localization system: Apply to smartphones. IEEE Transactions on Industrial Electronics pp. 1–1.

Yu, C., Lan, H., Gu, F., Yu, F. and El-Sheimy, N., 2017. A map/ins/wi-fi integrated system for indoor location-based service applications. Sensors.

Zhuang, Y. and El-Sheimy, N., 2016. Tightly-coupled integration of wifi and mems sensors on handheld devices for indoor pedestrian navigation. IEEE Sensors Journal 16(1), pp. 224–234.

Zhuang, Y., Hua, L. C., Wang, Q., Cao, Y., Gao, Z. Z., Qi, L. N., Yang, J. and Thompson, J., 2019. Visible light positioning and navigation using noise measurement and mitigation. IEEE Transactions On Vehicular Technology 68(11), pp. 11094–11106.

Zhuang, Y., Li, Y., Qi, L., Lan, H., Yang, J. and El-Sheimy, N., 2016. A two-filter integration of mems sensors and wifi fingerprinting for indoor positioning. IEEE Sensors Journal 16(13), pp. 5125–5126.